Resilience and Sustainability of Cities in Hazardous Environments
GVES, Napoli – New York, ISBN 978-88-903183-1-3

GLOBAL VOLCANIC SIMULATOR
Assessment of Multiple Hazards of Cities on Volcanoes

Flavio Dobran*

GVES
Global Volcanic and Environmental Systems Simulation
Napoli, Italy – New York, USA

Abstract. Global Volcanic Simulator is a physical–chemical–mathematical–computer model useful for assessing multiple hazards from volcanic eruptions and consists of the sub-models of the characteristic parts of volcanoes (magma chamber where magma accumulates and differentiates before erupting, volcanic conduit along which magma ascends to the surface, conduit surroundings, atmosphere above the surface of the volcano). For each volcanic eruption scenario, the simulator models are assembled by a scheduler and this scheduling is dynamic, since during an eruption different models of the same characteristic part of the volcano must be employed to account for the relevant volcanic processes. Each sub-model is properly verified and validated before being incorporated into the simulator, and many simulation scenarios must be used for multi-hazard assessment to ensure that the hazards associated with the environment surrounding a volcano are known with minimal uncertainties. This work summarizes the generalized model used in the simulator and the results of some simulations of magma chamber dynamics, magma ascent in volcanic conduits, and distribution of volcanic material in the atmosphere from a collapsing volcanic column at Vesuvius. The general multicomponent, multiphase, and three-dimensional transient model and more simpler models incorporated into the Global Volcanic Simulator are necessary for properly assessing multiple hazards of cities threatened by volcanic eruptions.

Keywords: Global Volcanic Simulator, Vesuvius, Vesuvio, Campi Flegrei, Phlegraean Fuelds, volcanoes, multiphase modeling, computer simulation, hazard assessment

1. Introduction

Volcanoes are fractures in the Earth's crust that allow magma, or partially molten silicate materials containing dissolved gases, to escape from the mantle. The Earth's composition is different in different parts of the crust and mantle and a wide variety of eruption modes is possible because of the complicated

* Corresponding author: dobran@gvess.org

interrelationships between the chemical and physical properties of these materials. The magma accumulating below a volcano in a mushy region called magma reservoir or magma chamber[1] changes composition from the assimilation with magma from deeper regions of the mantle and as it rises due to buoyancy its dissolved gases (largely water and carbon dioxide) exsolve and can generate great volumes of gases that upon exiting from a volcanic conduit produce high rising volcanic columns of gas and ash. When magma slowly degases during its ascent to the surface it produces slowly moving lava flows on the surface of the volcano. Magmas with large contents of dissolved gases fragment instead in the conduit and the resulting volcanic cloud or column reaches the stratosphere and then propagates laterally, transporting the material over the continents and possibly affecting the Earth's climate. As an eruption proceeds and heavier magma from the mantle is drawn toward the surface, the eruption column can collapse and produce ground-hugging pyroclastic flows which can move in excess of several hundred kilometers per hour and at high temperatures. The pyroclastic flow phase of an eruption is extremely dangerous and no living being can survive if caught in its wake [1].

The earth scientists studying volcanoes have been successful in mapping their locations or answering the "where" question [2], have been marginally successful in understanding "how" the eruptions develop, and have been unsuccessful in predicting "when" the eruptions will occur [3]. This lack of prediction presents problems for the cities on or close to the volcanoes, because without knowing the "when" of eruptions it is impossible to plan well in advance the evacuations of hundreds of thousands or millions of people that could be affected by the eruptions [4]. An alternative is to cohabit with volcanoes, but then it is necessary to produce resilient and sustainable habitats for the people in order to minimize the effects of eruptions. This interdisciplinary and transdisciplinary undertaking is, however, difficult to achieve, because it requires collaborations of actors with different interests and development of appropriate volcanic eruption scenarios in order to properly protect these habitats [5].

Volcanic earthquakes are caused by the fracturing of rocks from the changes of magma's composition and physical properties during its ascent through the mantle and lithosphere. Lava flows moving along the surface of a volcano are produced from the degassed magma exiting from the volcanic vent, and ash fall and pyroclastic flows are produced from the eruption column. Large pieces of rocks from the destruction of the volcanic edifice can also be produced and can reach the distances of tens of kilometers from the vent. Lahars are mixtures of water, ash, and gravel that travel along the valleys of the volcano and are produced from the condensation of water vapor in the eruption column. A single volcanic hazard or in combination with other hazards, such as ash fall, ejection of large pieces of rocks, and ground motions from earthquakes, can produce collapses of buildings in the built environment and severely damage the infrastructure. Pyroclastic flows hug the ground at high temperatures and cause asphyxiation

[1] Magma chamber contain partially molten rocks of different compositions and possibly gas bubbles from the exsolved gases.

problems and burns for living beings, and produce distributed loading forces and moments on structures [1, 6].

Assessments of multiple hazards of cities on active volcanoes require, therefore, the utilization of tools that can model different volcanic processes from the beginning to the end of eruptions. This requires accounting for chemical composition, storage and feeding characteristics of magma within the volcano, structure of volcanic edifice that may contain a variety of different fractured systems and aquifers, and condition of the built environment on the slopes of the volcano. Many of these parameters may, however, be poorly constrained and a large number of simulations is required: (1) to ascertain that the modeling equations are solved correctly, and (2) to assess the chemical and physical uncertainties associated with the models. The first task of *verification* must proceed the second task of *validation* and no single hazard assessment simulation can produce satisfactory results [7].

Building resilient and sustainable cities on volcanoes is, therefore, a complex undertaking where the simulation of different scenarios of volcanic eruptions must be performed by the tools that can adequately model the relevant volcanic processes. The premise of Global Volcanic Simulator [8, 9] is to accomplish this task and this integrative computer model is continuously being upgraded to ensure its usefulness. The current simulator can solve numerically the multidimensional forms of multicomponent and multiphase mass, momentum, energy, and entropy transport equations for each characteristic part of a volcano (magma chamber, volcanic conduit, surroundings of conduit and magma chamber, environment above the volcanic edifice) with the appropriate constitutive equations that best describe the material response (thermo-fluid and elasto-plastic deformations) of each part [1, 10, 11]. The coupling or boundary conditions for each part are being managed by a scheduler to ensure that each model of the simulator is being provided with the necessary boundary conditions to initiate its computational cycle. When a modeling part of the simulator needs boundary conditions for the execution of its next computational cycle and these conditions are not available before other parts execute their calculations, the scheduler places on hold the execution of this part until its boundary conditions become available (Fig. 1).

In the following, we will first summarize a generalized model of multiphase and multicomponent mixtures used in the simulator to produce models for different parts of the volcanic system. Some of these parts can be modeled with simple models whereas others require very complex modeling strategies in order to properly account for the variety of volcanic processes occurring during an eruption. The simple models presented pertain to the long-term (hundreds to thousands of years) magma supply and discharge from magma chambers and short-term (days to months) magma ascent along the conduits. Modeling of eruption columns requires the use of complex three-dimensional multiphase and multicomponent models. The details of the physical–chemical–mathematical equations used in the simulator for modeling volcanic processes can be found elsewhere [1, 10] and are not described herein. Each model employed requires verification and valida-

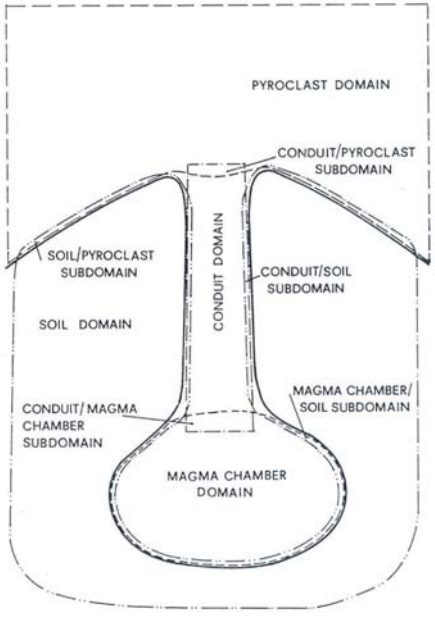

(a) Schematic illustration of the decomposition of volcano into different parts or domains.

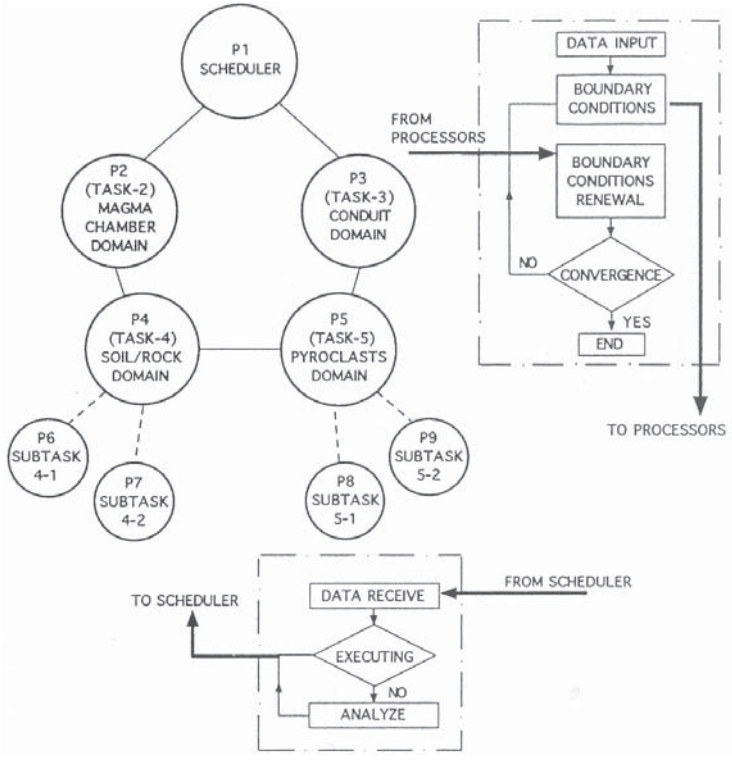

(b) Computer implementation for the interaction and scheduling computations within the domains.

Figure 1. Global Volcanic Simulator architecture. Subdomains exchange boundary conditions between domains and the entire computation is performed in a multiprocessor environment on one or more computers connected in a network [8, 9, 12].

tion, in the sense that its physical–chemical–mathematical equations are solved with an acceptable numerical accuracy by conducting grid-size and time-step refinements, and use of most effective modeling strategy.

2. Generalized Multiphase and Multicomponent Material Transport Model

2.1 Eulerian Form of Material Transport Laws

The physical laws governing the transport of mass, momentum, and energy of multicomponent and multiphase Eulerian phases can be established through formal averaging procedures involving the well–established single–phase macroscopic transport model of matter [10]. The averaging procedure acts like a filter which eliminates detailed tracking of matter particles while allowing for their gross motions and interactions. The volume averaging is most useful, for it not only furnishes the desired mass, momentum, energy, and entropy transport laws for each phase of a multiphase mixture, but also provides an additional set of transport equations that account for the structural properties of the mixture, such as the size of the averaging region and the information associated with the averaging process. A structural model of multiphase mixtures also eliminates the complications associated with turbulence modeling based on the Reynolds averaging procedures of single–phase flows and parallels that of large eddy simulation where only the local turbulence scales are averaged while the large scales are computed.

Structural properties of multiphase mixture include particle inertia, rotation, and dilatancy (expansion–contraction effects), and can be directly associated with turbulence production and dissipation. The structural effects of multiphase mixtures are intimately tied with the microphysical processes at the centimeter and smaller scales where the turbulent energy is dissipated and thus contribute to the global plume dynamics where this energy is produced.

When the pyroclastic dispersion models do not account for a systematic coupling between different turbulence scales they fail in their predictive capabilities for modeling long–duration and high–rising volcanic plumes. Turbulence is ubiquitous in volcanic plumes and no serious attention has been paid to date to the effects of large turbulence Reynolds numbers on energy dissipation, coupling between small and large scales of turbulence, effects of Stokes number or particle size, particle loading, volume fraction, particle settling parameter, and the relative importance of viscous, inertia, and buoyancy forces [11].

In the structured model of multiphase mixtures, a macroscopic averaging volume U contains all phases of the mixture and the local thermodynamic properties F^α of phase α appear as *volume–averaged* variables

$$< F^\alpha >= \frac{1}{U_\alpha} \int_{U_\alpha} F^\alpha \, dU \tag{1}$$

where U_α is the volume of phase α in U.

The *density–weighted average* F_α, *partial average* $\bar{F}_\alpha$, and *phase average* $\bar{\bar{F}}_\alpha$ are defined as

$$F_\alpha = \frac{<\rho^\alpha F^\alpha>}{<\rho^\alpha>} = \frac{1}{\bar{\rho}_\alpha}\frac{U_\alpha}{U} <\rho^\alpha F^\alpha> \tag{2}$$

$$\bar{F}_\alpha = \frac{U_\alpha}{U} <F^\alpha>, \qquad \bar{\bar{F}}_\alpha = <F^\alpha> \tag{3}$$

The *partial density of phase* α denotes the mass of phase α per unit volume of mixture and is defined by

$$\bar{\rho}_\alpha = \frac{U_\alpha}{U} <\rho^\alpha> = \phi_\alpha \bar{\bar{\rho}}_\alpha, \quad \bar{\rho} = \sum_{\alpha=1}^{\gamma} \bar{\rho}_\alpha \tag{4}$$

where ϕ_α is the *volume fraction* (U_α/U), $\bar{\bar{\rho}}_\alpha$ is the volume–averaged mass density of phase α in the averaging volume, and $\bar{\rho}$ is the *density of the multiphase mixture*.

The *velocity of phase* α, $\mathbf{v}_\alpha$, and the *mixture velocity*, $\mathbf{v}$, are defined as

$$\mathbf{v}_\alpha = \frac{1}{\bar{\rho}_\alpha}\frac{U_\alpha}{U} <\rho^\alpha \mathbf{v}^\alpha>, \qquad \mathbf{v} = \frac{1}{\bar{\rho}} \sum_{\alpha=1}^{\gamma} \bar{\rho}_\alpha \mathbf{v}_\alpha \tag{5}$$

and the *diffusion velocity* of phase α, $\mathbf{u}_\alpha$, is the velocity relative to the center of mass and satisfies

$$\mathbf{u}_\alpha = \mathbf{v}_\alpha - \mathbf{v}, \qquad \sum_{\alpha=1}^{\gamma} \bar{\rho}_\alpha \mathbf{u}_\alpha = 0 \tag{6}$$

By employing the above definitions, the averaging procedure produces the following expression for the *balance of mass of phase* α

$$\grave{\bar{\rho}}_\alpha + \bar{\rho}_\alpha \boldsymbol{\nabla}\cdot\mathbf{v}_\alpha = \hat{c}_\alpha = -\frac{1}{U}\int_{a^\Lambda} m^\alpha da \tag{7}$$

where the backward prime affixed to a phase variable denotes the *material derivative* following that phase. The mass generation rate per unit volume of the mixture $\hat{c}_\alpha$ arises from the phase change processes, a^Λ denotes the interfacial area of phase α in U, m^α is the local mass transfer rate across the interface, and $\hat{c}_\alpha$ is equal to zero if there is no mass transfer across the interfaces.

The conservation of mass for a *multiphase mixture* is obtained by summing from $\alpha = 1$ to $\alpha = \gamma$ in Eq. (7). This produces

$$\frac{\partial\bar{\rho}}{\partial t} + \boldsymbol{\nabla}\cdot\bar{\rho}\mathbf{v} = 0 \quad \text{or} \quad \dot{\bar{\rho}} + \bar{\rho}\boldsymbol{\nabla}\cdot\mathbf{v} = 0, \qquad \sum_{\alpha=1}^{\gamma} \hat{c}_\alpha = 0 \tag{8}$$

where the third equation accounts for the mass conservation property of the mixture and the dot over the mixture density signifies the *material derivative* following the motion of the mixture as a whole.

The *linear momentum of phase* α is expressed by

$$\bar{\rho}_\alpha \grave{\mathbf{v}}_\alpha = \boldsymbol{\nabla}\cdot\bar{\mathbf{T}}_\alpha + \bar{\rho}_\alpha \mathbf{b}_\alpha + \hat{\mathbf{p}}_\alpha \tag{9}$$

where $\bar{\mathbf{T}}_\alpha$ is the stress tensor and $\mathbf{b}_\alpha$ is the body force per unit mass. $\hat{\mathbf{p}}_\alpha$ is the momentum source per unit volume and arises from phase changes and structural effects of the mixture because of the finite size of the averaging volume U.

The *angular momentum of phase* α expresses the non-symmetry of the stress tensor

$$\mathbf{M}_\alpha = \bar{\mathbf{T}}_\alpha - \bar{\mathbf{T}}_\alpha^T \tag{10}$$

where the superscript T denotes transpose. This asymmetry can be produced by particle spins, couple stresses, and body moments.

The *conservation of energy of phase* α takes the following form

$$\bar{\rho}_\alpha \grave{\bar{\varepsilon}}_\alpha = \mathrm{tr}(\bar{\mathbf{T}}_\alpha^T\cdot(\boldsymbol{\nabla}\mathbf{v}_\alpha)) - \boldsymbol{\nabla}\cdot\bar{\mathbf{q}}_\alpha + \bar{\rho}_\alpha r_\alpha + \hat{\epsilon}_\alpha \tag{11}$$

where ε_α is the internal energy, tr denotes the trace operation, r_α is the energy generation rate per unit mass, and $\hat{\epsilon}_\alpha$ accounts for both the energy transfer rate per unit volume between the phases and the structural properties of the mixture.

The *entropy inequality of phase* α satisfies

$$\bar{\rho}_\alpha \grave{\bar{s}}_\alpha + \boldsymbol{\nabla}\cdot\left(\frac{\bar{\mathbf{q}}_\alpha}{\bar{\bar{\theta}}_\alpha}\right) - \frac{\bar{\rho}_\alpha r_\alpha}{\bar{\bar{\theta}}_\alpha} + \hat{c}_\alpha s_\alpha + \hat{s}_\alpha \geq 0 \tag{12}$$

where s_α is the entropy, $\bar{\bar{\theta}}_\alpha$ is the *phase averaged temperature*, and $\hat{s}_\alpha$ is the *entropy source of phase* α that is not necessarily positive semidefinite.

The phasic conservation of mass, linear and angular momenta, energy, and entropy Eqs. (7, 9-12) are similar to the corresponding equations of single–phase multicomponent mixtures and reduce to the latter if the interfacial effects of the mixture are negligible. Every physically consistent theory of multiphase mixtures should have such a *consistency property* in order to reproduce at least the most simple and known physical phenomena.

The motion of each phase relative to the center of mass is accounted for by taking moments of the phasic conservation of mass and momentum equations *relative to the center of mass*. These operations produce the *balance of equilibrated inertia*

$$\bar{\rho}_\alpha \grave{i}_\alpha = -\hat{c}_\alpha(i_\alpha - \hat{i}_\alpha) + 2\bar{\rho}_\alpha i_\alpha \frac{\grave{\phi}_\alpha}{\phi_\alpha} - \boldsymbol{\nabla}\cdot\left(\mathbf{U}_\alpha \frac{\grave{\phi}_\alpha}{\phi_\alpha}\right) \tag{13}$$

and *balance of equilibrated moments*

$$\begin{aligned}\bar{\rho}_\alpha i_\alpha \overline{\grave{\frac{\phi_\alpha}{\phi_\alpha}}} = &-\hat{c}_\alpha \frac{\grave{\phi}_\alpha}{\phi_\alpha}(i_\alpha - \hat{i}_\alpha) + \bar{S}_\alpha + \boldsymbol{\nabla}\cdot\bar{\boldsymbol{\lambda}}_\alpha - \bar{\rho}_\alpha i_\alpha \frac{\grave{\phi}_\alpha}{\phi_\alpha}\boldsymbol{\nabla}\cdot\mathbf{v}_\alpha \\ &+\bar{\rho}_\alpha i_\alpha \left(\frac{\grave{\phi}_\alpha}{\phi_\alpha}\right)^2 - \left(\frac{\grave{\phi}_\alpha}{\phi_\alpha}\right)\boldsymbol{\nabla}\cdot\left(\mathbf{U}_\alpha \frac{\grave{\phi}_\alpha}{\phi_\alpha}\right)\end{aligned} \tag{14}$$

where the *isotropic inertia of phase* α is defined as

$$i_\alpha = \frac{1}{\bar{\rho}_\alpha}\frac{1}{U}\int_{U_\alpha} \rho^\alpha \boldsymbol{\xi}\cdot\boldsymbol{\xi}\, dU \tag{15}$$

with $\boldsymbol{\xi}$ is the position vector relative to the center of mass. In the equilibrated inertia equation, $\hat{i}_\alpha$ represents the source of inertia due to phase change, whereas $\mathbf{U}_\alpha$ accounts for triple correlations of $\boldsymbol{\xi}$ which are associated with the non-uniformities within the averaging volume. The moment of surface forces acting on the surface of volume U_α in U is represented in the equilibrated moments equation by $\bar{S}_\alpha$, whereas $\bar{\boldsymbol{\lambda}}_\alpha$ in this expression represents the volume–averaged moment of the stress tensor $\bar{\mathbf{T}}_\alpha$.

The above multiphase material transport equations are the result of replacing continuous distribution of forces in the averaging volume by the resultant forces and couples acting on this volume. When the forces acting on the surface of U_α are averaged, the result is an average force which is represented by the surface traction force $\bar{\mathbf{T}}_\alpha\cdot\mathbf{n}_\alpha$ and a resultant couple represented by $\bar{\mathbf{S}}_\alpha$. Similarly, the average stress tensor $\bar{\mathbf{T}}_\alpha$ and intrinsic stress moment $\bar{\boldsymbol{\lambda}}_\alpha$ replace the local variation of stress tensor within U_α. These results are consistent with particle mechanics where the forces acting on a collection of particles can be replaced by a resultant force and a resultant couple. The structural properties of the mixture are thus accounted for by i_α, $\mathbf{U}_\alpha$, $\bar{\mathbf{S}}_\alpha$, and $\bar{\boldsymbol{\lambda}}_\alpha$, and may also appear in the phasic variables $\bar{\mathbf{T}}_\alpha$, $\hat{\mathbf{p}}_\alpha$, $\bar{\mathbf{q}}_\alpha$, $\hat{i}_\alpha$, $\hat{\epsilon}_\alpha$, and $\hat{c}_\alpha$. These variables are required to satisfy certain constitutive principles and the second law of thermodynamics as represented by Eq. (12).

When some of the results of constitutive theory of mixtures of fluids [10] are used in the above transport equations, these expressions, expressed in the tensor index notation with indices i, j, and k, reduce to the following forms:

Conservation of Mass:

$$\frac{\partial\bar{\rho}_\alpha}{\partial t} + \frac{\partial\bar{\rho}_\alpha v_{\alpha j}}{\partial x_j} = \hat{c}_\alpha, \qquad \bar{\rho}_\alpha = \phi_\alpha\bar{\bar{\rho}}_\alpha \tag{16}$$

$$\frac{\partial\bar{\bar{\rho}}_\alpha}{\partial t} + \frac{\partial\bar{\bar{\rho}}_\alpha v_{\alpha j}}{\partial x_j} = \frac{\hat{c}_\alpha}{\phi_\alpha} - \bar{\bar{\rho}}_\alpha\varphi_\alpha, \qquad \varphi_\alpha = \frac{\dot{\phi}_\alpha}{\phi_\alpha} \tag{17}$$

Conservation of Momentum:

$$\begin{aligned}\frac{\partial\bar{\rho}_\alpha v_{\alpha i}}{\partial t} + \frac{\partial\bar{\rho}_\alpha v_{\alpha i}v_{\alpha j}}{\partial x_j} &= -\phi_\alpha p_{\alpha,i} - \frac{1}{2}\bar{\rho}_\alpha i_\alpha\left(\frac{\dot{\phi}_\alpha}{\phi_\alpha}\right)^2_{,i} + \left(O_{\alpha\alpha}\phi_\alpha\frac{\dot{\phi}_\alpha}{\phi_\alpha}\right)_{,i}\\ &+\hat{c}_\alpha v_{\alpha i} + \left[\lambda_{\alpha\alpha}\, D_{\alpha kk}\delta_{ij} + 2\,\mu_{\alpha\alpha}D_{\alpha ij} + 2\,\bar{\rho}_\alpha C_\alpha\phi_{\alpha,i}\phi_{\alpha,j}\right]_{,j}\\ &- \sum_\beta^{\gamma-1}\xi_{\alpha\beta}(v_{\beta i} - v_{\gamma i}) - \sum_\beta^{\gamma}\gamma_{\alpha\beta}\bar{\bar{\theta}}_{\beta,i} - \sum_\beta^{\gamma}\Delta_{\alpha\beta}\bar{\bar{\rho}}_{\beta,i} + \bar{\rho}_\alpha b_{\alpha i}\end{aligned} \tag{18}$$

where $D_{\alpha ij}$ is the deformation rate tensor, and an index following a comma in a subscripted variable denotes the partial derivative with respect to that index; for example, $p_{\alpha,i} = \partial p_\alpha / \partial x_i$. In Eq. (18), p_α is the thermodynamic pressure, $\lambda_{\alpha\alpha}$ and $\mu_{\alpha\alpha}$ are the bulk and shear viscosity coefficients, respectively, C_α and $O_{\alpha\alpha}$ are structural property coefficients, $\xi_{\alpha\beta}$ are viscous drag coefficients, $\gamma_{\alpha\beta}$ are Soret effect coefficients, and $\Delta_{\alpha\beta}$ are density gradient coefficients. The viscosity coefficients include both viscous and turbulent contributions and the latter can be modeled with the subgrid scale models. The stress term with the parameter C_α accounts for Mohr–Coulomb yield–type criteria of plastic deformation when the volume fraction gradients become high and the flow begins to creep as in pyroclastic flows during material sedimentation. In this situation, the pressure gradient becomes balanced by the gravity and compaction characteristics of particulates. This stress term thus accounts for the yield stress of the material and is independent of the rate of strain. It produces energy dissipation (see Eq. (20) below).

Conservation of Total Energy:

One can derive several useful forms for the energy equation. The one that we will need is the total energy equation for phase α, which is obtained by adding the scalar product of velocity and momentum Eq. (9) to the internal energy Eq. (11). By defining the total energy of phase α as being the sum of internal, kinetic, and compaction energies, i.e.

$$e_\alpha = \varepsilon_\alpha + \frac{1}{2} v_{\alpha i} v_{\alpha i} + C_\alpha \phi_{\alpha,i} \phi_{\alpha,i} \tag{19}$$

The conservation equation for total energy of phase α thus becomes,

$$\begin{aligned}
\frac{\partial \bar{\rho}_\alpha e_\alpha}{\partial t} + \frac{\partial \bar{\rho}_\alpha e_\alpha v_{\alpha j}}{\partial x_j} &= -\bar{q}_{\alpha i,i} - \phi_\alpha (p_\alpha v_{\alpha i})_{,i} + (O_{\alpha\alpha} \phi_\alpha \varphi_\alpha v_{\alpha i})_{,i} \\
&\quad + \left[(\lambda_{\alpha\alpha}\, D_{\alpha kk} \delta_{ij} + 2\, \mu_{\alpha\alpha} D_{\alpha ij} + 2\, \bar{\rho}_\alpha C_\alpha \phi_{\alpha,i} \phi_{\alpha,j})\, v_{\alpha i} \right]_{,j} \\
&\quad - v_{\alpha i} \sum_\beta^{\gamma-1} \xi_{\alpha\beta} (v_{\beta i} - v_{\gamma i}) - v_{\alpha i} \sum_\beta^{\gamma} \gamma_{\alpha\beta} \bar{\bar{\theta}}_{\beta,i} - v_{\alpha i} \sum_\beta^{\gamma} \Delta_{\alpha\beta} \bar{\bar{\rho}}_{\beta,i} \\
&\quad + \bar{\rho}_\alpha b_{\alpha i} v_{\alpha i} + \bar{\rho}_\alpha r_\alpha - \bar{q}_{s\alpha} + \hat{c}_\alpha (\hat{\epsilon}_\alpha + \frac{1}{2} v_{\alpha i} v_{\alpha i} + C_\alpha \phi_{\alpha,i} \phi_{\alpha,i}) \\
&\quad - \phi_\alpha \varphi_\alpha (p_\alpha - \beta_\alpha) - v_{\alpha i} \frac{1}{2} (\varphi_\alpha^2)_{,i}\, \bar{\rho}_\alpha \dot{i}_\alpha
\end{aligned} \tag{20}$$

In this equation $\bar{q}_{s\alpha}$ is the interfacial heat transfer rate per unit volume, whereas the *configuration pressure* β_α can be computed from the Helmholtz potential. This pressure arises from the changes in the packing of phase α and thus reflects the strength of contact forces between this and other phases. A reasonable choice for this pressure is the packing stress of material grains.

The total energy Eq. (20) shows how the energy of each phase is distributed between different processes. The convection of energy is balanced by heat transfer

due to temperature gradients within the phases, temperature differences between the phases, phase changes releasing or requiring latent heat, viscous dissipation which produces heat from fluid friction within each phase and from the exchange of momenta between the phases, flow work associated with pressure and distribution of phases, energy generation from electromagnetic or other processes, and the work expended in distributing phase matter in different regions of vorticity. The larger the phase inertia and its volume fraction gradient, the more energy from large eddies must be expended or dissipated by the small eddies to maintain equilibrium. The strengths of contact forces between the phases and the phasic dilatation rates can both produce and dissipate energy within a mixture. The redistribution of particulate and non–particulate matter at small scales is thus governed by phase inertia, volume fraction (particle loading), and configuration pressure parameters.

Inertia Transport Equation:

$$\frac{\partial \bar{\rho}_\alpha i_\alpha}{\partial t} + \frac{\partial \bar{\rho}_\alpha i_\alpha v_{\alpha j}}{\partial x_j} = \hat{c}_\alpha \hat{i}_\alpha + 2\,\bar{\rho}_\alpha i_\alpha \varphi_\alpha - (\varphi_\alpha U_{\alpha m})_{,m} \tag{21}$$

Dilatation–Contraction Transport Equation:

$$\frac{\partial \bar{\rho}_\alpha \varphi_\alpha}{\partial t} + \frac{\partial \bar{\rho}_\alpha \varphi_\alpha v_{\alpha j}}{\partial x_j} = \hat{c}_\alpha \varphi_\alpha - D_{\alpha kk}(\bar{\rho}_\alpha \varphi_\alpha + \frac{\phi_\alpha}{i_\alpha} O_{\alpha\alpha}) + \frac{1}{i_\alpha} \sum_{\beta}^{\gamma} (\kappa_{\alpha\beta} i_\beta + H_{\alpha\beta} \phi_\beta \varphi_\beta) - \bar{\rho}_\alpha \varphi_\alpha^2 \tag{22}$$

The inertia and dilatation–contraction transport equations account for small scale effects in the flow, which have been averaged out through the averaging procedure of local mass, momentum, and energy transport laws. In our model, the microstructural effects survive through phase inertia, volume fraction, and configuration pressure, and provide a feedback to the mean flow. The phase inertia can be viewed as a measure of turbulent intensity and $U_{\alpha m}$ as proportional to the gradient of this intensity.

Since the phase inertia moderates both the production of turbulent kinetic energy and turbulent dissipation rate, the inertia transport Eq. (21) can be split into two interacting parts that model this turbulence. The size of the averaging volume can be, therefore, interpreted as the filter width, with the microstructural parameters defining its characteristics. The resulting structural model is thus analogous to large eddy simulation models where the small scales are averaged out and modeled and the large ones are computed. It is also considerably simpler than the multiphase flow turbulence models based on the single–phase flow Reynolds averaging where there are too many poorly constrained modeling parameters.

To close the above equations we also need a constitutive equation for the heat flux rate, which in linearized form can be written as

$$\bar{q}_{\alpha i} = -\sum_{\beta}^{\gamma} \kappa_{\alpha\beta} \bar{\bar{\theta}}_{\beta,i} - \sum_{\beta}^{\gamma} \nu_{\alpha\beta} \bar{\bar{\rho}}_{\beta,i} - \sum_{\beta}^{\gamma-1} \varsigma_{\alpha\beta}(v_{\beta i} - v_{\gamma i}) - \sum_{\beta}^{\gamma} \Gamma_{\alpha\beta} \phi_{\beta,i} \quad (23)$$

where the first term on the right represents the Fourier effect (heat flow due to temperature gradients) and the second term is the Dufour effect (heat flow due to mass transfer). Except for the temperature gradient term in this equation, all other terms can, in general, be neglected. Equation (12) places restrictions on the phenomenological coefficients of constitutive equations and requires that the following conditions be satisfied

$$\kappa_{\alpha\alpha} \geq 0; \qquad H_{\alpha\alpha} \geq 0; \qquad O_{\alpha\alpha} \leq 0; \qquad \lambda_{\alpha\alpha} + \frac{2}{3}\mu_{\alpha\alpha} \geq 0;$$
$$\xi_{\alpha\alpha} \geq 0; \qquad \xi_{\alpha\beta} \leq 0, \qquad \alpha \neq \beta \neq \gamma \quad (24)$$

The interfacial heat transfer can be modeled as

$$\bar{q}_{s\alpha} = \bar{h}_{\alpha}(\bar{\bar{\theta}}_{\alpha} - \bar{\bar{\theta}}_{g}) \quad (25)$$

where $\bar{\bar{\theta}}_g$ is the temperature of the gas phase and $\bar{h}_\alpha$ is the heat transfer coefficient. The phase change energy flux $\hat{c}_\alpha \hat{\hat{e}}_\alpha$ is related to the mass supply $\hat{c}_\alpha$ and average energy of interfaces of phase α. Similarly, the source of inertia $\hat{c}_\alpha \hat{i}_\alpha$ is related to the mass supply and average inertia of interfaces of phase α. Modeling of $\hat{c}_\alpha$ depends on the composition and chemical reactions of the constituents of phase α, and, in order to account for these effects, we must extend the single–component multiphase flow theory to one involving many components. This extension is discussed in the following section.

2.2 Multiphase–Multicomponent Flows

While it is possible to assign unique properties to each chemical constituent or component in a mixture, we will not follow this approach in order to keep the model as simple as possible. In our approximation, we only modify the conservation of mass equation of each phase to account for the diffusion of each constituent and retain the previously–derived phasic conservation equations for momentum, energy, inertia, and dilatation–contraction transport.

If $\omega_{a\alpha}$ is the mass fraction of constituent a in phase α, Eqs. (7) and (8) can be used to show

$$\frac{\partial \bar{\rho}_\alpha \omega_{a\alpha}}{\partial t} + \frac{\partial \bar{\rho}_\alpha \omega_{a\alpha} v_{\alpha j}}{\partial x_j} = \hat{c}_{a\alpha} - \frac{\partial J_{a\alpha j}}{\partial x_j}; \quad a = 1, \cdots, s \quad (26)$$

$$\frac{\partial \bar{\bar{\rho}}_\alpha \omega_{a\alpha}}{\partial t} + \frac{\partial \bar{\bar{\rho}}_\alpha \omega_{a\alpha} v_{\alpha j}}{\partial x_j} = \frac{\hat{c}_{a\alpha}}{\phi_\alpha} - \bar{\bar{\rho}}_\alpha \varphi_\alpha - \frac{1}{\phi_\alpha} \frac{\partial J_{a\alpha j}}{\partial x_j}; \quad a = 1, \cdots, s \quad (27)$$

where $\hat{c}_{a\alpha}$ is the net mass generation rate per unit volume and $\mathbf{J_{a\alpha}}$ is the *mass diffusion flux* of constituent a in phase α. $\hat{c}_{a\alpha}$ accounts for the combined effects of nucleation, condensation, evaporation, aggregation, fragmentation, and chemical reactions. The constituent mass generation rate is equal to zero if no constituent is produced or consumed, while its mass flux can be produced with or without chemical reactions. Conservation of mass of each chemical constituent then requires

$$\sum_{a=1}^{s} \omega_{a\alpha} = 1, \quad \alpha = 1, \cdots, \gamma; \quad \sum_{a=1}^{s} \hat{c}_{a\alpha} = \hat{c}_{\alpha}, \quad \sum_{\alpha=1}^{\gamma} \hat{c}_{\alpha} = 0 \tag{28}$$

The diffusion flux $\mathbf{J_{a\alpha}}$ accounts for the diffusion of component a relative to the mean flow of phase α and, according to the kinetic theory [13], is proportional to the mass fraction gradient

$$\mathbf{J}_{a\alpha} = -\mathbf{K_{a\alpha}} \cdot \boldsymbol{\nabla} \omega_{\mathbf{a}\alpha} \tag{29}$$

where $\mathbf{K_{a\alpha}}$ is the *mass diffusion tensor* that accounts for the effects of turbulence.

The Eulerian formalism is useful for modeling the continuous gas phase and large number of fine particulate phases of the mixture because these strongly interact with each other through collisions and turbulence. The centimeter-size and larger particles are affected much less by the gas and small particulate motions and tend to follow the ballistic trajectories. Their motions are more effectively described by the Lagrangian kinetic equations which we will not present in this work, but are available in the simulator for simultaneously modeling the continuous and discrete phases.

2.3 Generalized Model Implementation

The generalized multiphase and multicomponent transport theory model discussed above can be simplified by neglecting certain processes through the appropriate use of *nondimensional analysis* [1] or by averaging over one or more spatial dimensions when the variations of physical variables in these dimensions are not as significant as in other spatial dimensions. Opening of volcanic conduits and magma ascent in conduits can sometimes satisfy these requirements and are often better approximations of physical phenomena than the more complex models where the specifications of some parameters becomes highly uncertain. The choice of appropriate models in the Global Volcanic Simulator requires considerable similarity with modeling strategies, because the mere use of models propagated through computer codes and without understanding their limitations does not produce an understanding of the modeled processes.

3. Global Volcanic Simulator Models

Global Volcanic Simulator employs different models based on the generalized model discussed above [1, 10, 14] to model the material transport in the vol-

canic system, where each part of this system (magma chamber, conduit, atmosphere) employs the relevant thermal, fluid mechanics, and mechanical constitutive equations to account for fluid- and solid-like material behaviors. The generalized model can account for very complex volcanic processes occurring in volcanic columns and magma chambers, and can be simplified to simpler situations involving steady-state, one-dimensional, or lumped parameter situations, as illustrated by the following models of magma chamber dynamics, opening of volcanic conduit, magma ascent in conduit, and distribution of pyroclasts in the atmosphere above the volcano.

3.1 Magma Chamber Dynamics

The *magma chamber model* depicted in Fig. 2a considers the inner region of the chamber as a mixture of magma, solids, and gases, and the surrounding regions as thermoplastic and thermoelastic solids. This model allows for simulating the long-term subplinian and plinian activity of a volcano by accounting for magma supply from the mantle and opening of volcanic conduit when the pressure in the chamber exceeds the yield strength of the overlying rocks. An application of this model to Vesuvius (Fig. 2b,c), with magma chamber volume of about 10 km^3 and located at 5 km below the surface, shows the semi-cyclic eruptions of this volcano and suggests that the next eruption has a high probability of being plinian and not subplinian as assumed in the Vesuvius Evacuation Plan [4].

3.2 Magma Ascent in Conduits

The *conduit opening model* shown in Fig. 3a considers magma ascent along a one-dimensional fracture. Here magma rises because of buoyancy and its pressure decrease causes the exsolution of dissolved gases. Its ascent is controled by the Froude, Reynolds, and Magma Porosity numbers, where the small Reynolds and Magma Porosity numbers inhibit the ascent velocity through the conduit because of the small permeability of magma reservoir and high shearing stresses (from large magma viscosity), suggesting that an eruption will not occur until a certain critical amount of melt is available in the magma reservoir.

When the rising magma in a conduit begins exsolving gases (Fig. 3b) it is necessary to employ a different model that utilizes single phase flow in one part of the conduit and multiphase flow with gaseous phases in the more superficial part of the conduit. This more complicated model allows for the determination of pressure, temperature, velocities of phases, void fractions, and mass fractions at the conduit exit, which serve as the boundary conditions for the volcanic column model described below. Such a model accounts for magma fragmentation in a conduit and suggests that for very viscous magmas the magma pressure in a conduit can fall significantly below the lithostatic pressure of surrounding rocks and cause water from the aquifers to enter into the conduit. The resulting magma–water interaction produces a violent phreatomagmatic eruption capable of decapitating the entire cone of a volcano [1], as happened during the 1631 eruption of Vesuvius [16].

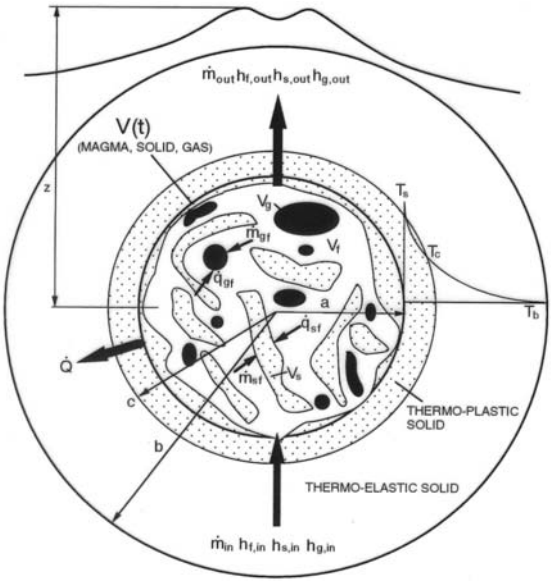

(a) Magma chamber with inner region consisting of melt, solids, and exsolved gases, and outer regions consisting of thermoplasic and thermoelastic solids.

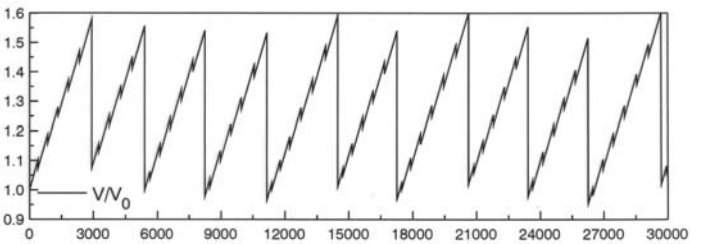

(b) Variation of magma chamber volume V with time.

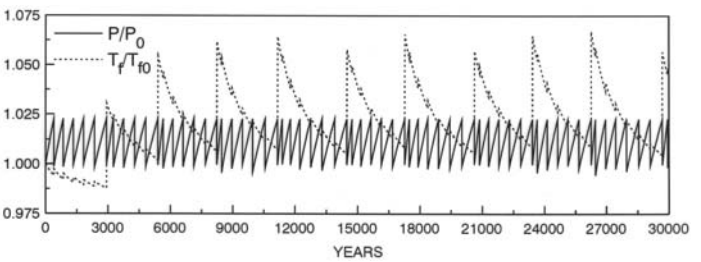

(c) Variations of magma chamber pressure P and temperature T_f with time.

Figure 2. Plinian eruptions of Vesuvius occur every few thousand years and subplinian eruptions occur every few centuries, as inferred from the studies of historical eruptions [15].

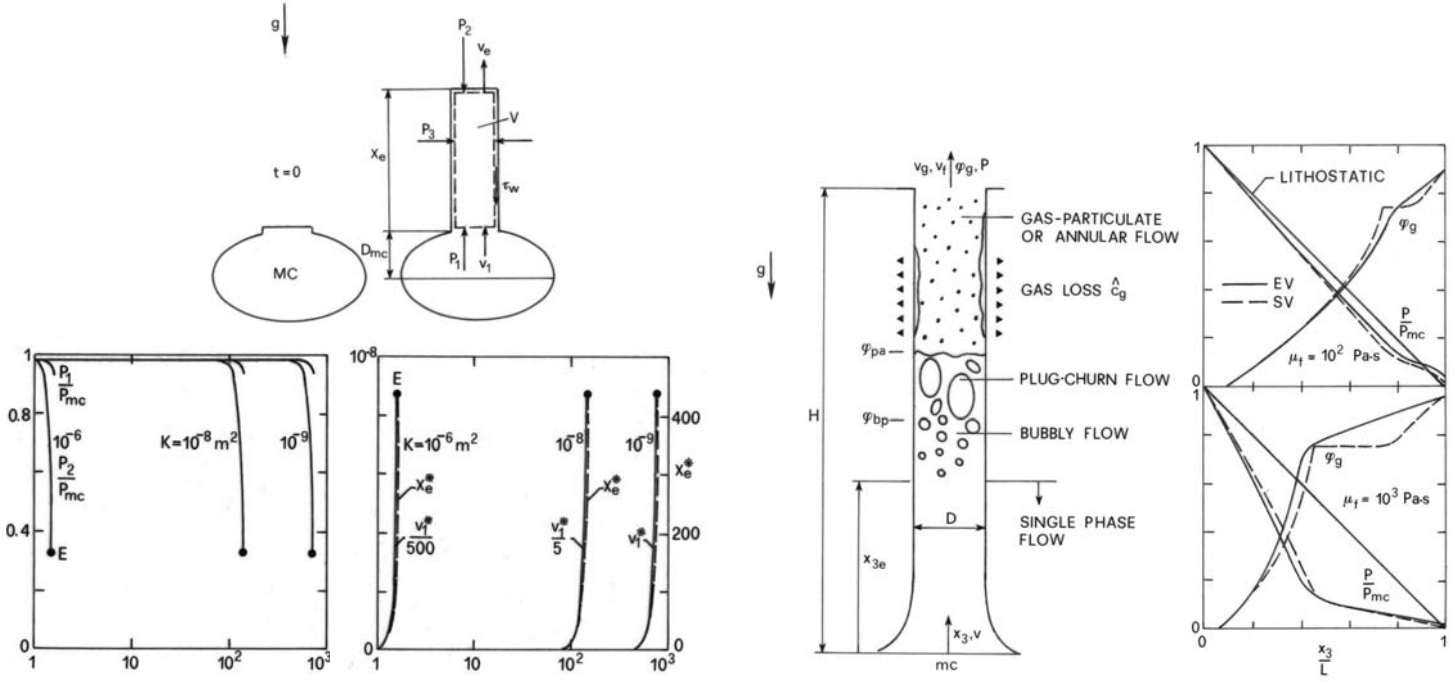

(a) One-dimensional single phase flow model of opening of volcanic conduit and distributions of magma front pressure P_2, velocity v_1, and distance x_e with time as a function of magma chamber permeability K. Ponts E are termination points of calculation, because the dissolved gases begin exsolving and the model becomes invalid.

(b) One-dimensional two-phase flow model of magma ascent in a conduit and vertical pressure P and gas volume fraction φ_g distributions, where P_{mc} and μ_f are magma chamber pressure and magma viscosity, respectively.

Figure 3. Opening of volcanic conduit and and magma ascent along the conduit.

3.3 Collapsing Volcanic Column

Time-dependent and three-dimensional simulation of a volcanic column is a very complex undertaking because the column consists of gaseous phases (air, water vapor, carbon dioxide), solid phases (different sizes of pyroclasts ranging from micron-size ash particulates to cm-size pieces of rock from the volcanic edifice), and nucleating and growing liquid water droplets (produced from the condensation of water vapor exsolved from magma during its ascent to the surface). Modeling of the condensation process in the atmosphere requires the consideration of microphysics of the process, which is currently incompletely understood as in weather predictions [11], and its neglect in the column is permissible when the column does not rapidly rises toward the tropopause where the air temperature reaches –60°C. This occurs when the column collapses in the troposphere close to the vent and produces pyroclastic flows that tend to hug the ground for tens of minutes before producing secondary columns that lift hot ash high into the atmosphere. The behavior of eruption column depends on the chemical and physical properties of the erupted material that during an eruption changes, since with time magmas with heavier compositions are erupted [1–3].

For assessing multiple hazards of an eruption with the built environment in the proximity of the volcano, multiple simulations must be performed with different volcano topographies and without and with this environment, and in the latter situation with sufficient grid resolutions that resolve significant human structures. Here, we will summarize the results of a simulation for Vesuvius that illustrates the necessity of defining the *exclusion area* around this volcano [5].

The topography of the volcano was produced from the 5 m resolution UTM data available from Istituto Geografico Militare Italiano and Fig. 4a shows a triangular grid of the topography around the cone of Vesuvius and Somma caldera used in calculations. The computational grid in the simulation includes the base area of 200 km^2 and the height of the troposphere, so that the collapsed volcanic column is fully contained in this volume during the entire duration of simulation. Figure 4b shows the temperature distribution of pyroclastic flows following the collapse of volcanic column and points to a very complex structure that does not only depend on the topography, but also by the thermo–fluid mechanics processes in the eruptive cloud, produced from the interactions of secondary columns above the pyroclastic flows.

The secondary columns above the pyroclastic flows are produced from the vertical buoyancy forces in the flows and cause continuous changes in the global column and limit the propagation distances of flows that are different in different directions. The hugging of the flows close to the central cone of the volcano suggests that the *exclusion nucleus* of this volcano has a limited extend of several kilometers from the vent and that outside of this area it should be possible to produce resilient and sustainable areas where the population can cohabit with the volcano. The redefinition of danger zones around Vesuvius and Phlegraean Campi Flegrei into exclusion nuclei, resilience belts, and sustainability areas is the key feature of VESUVIUS–CAMPIFLEGREI PENTALOGUE [5].

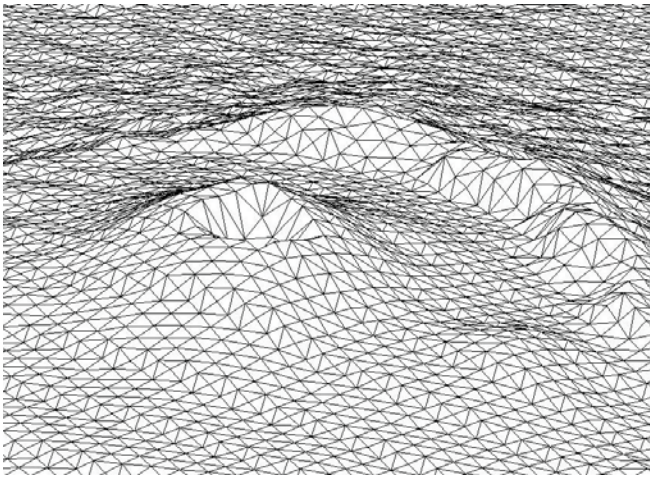

(a) Triangular grid of Somma–Vesuvius topography.

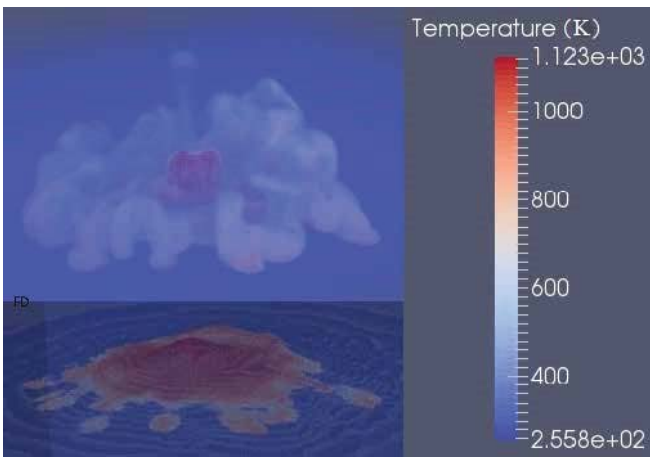

(b) Temperature distribution of pyroclastic flows on the surface and above the surface of volcano following the collapse of volcanic column.

Figure 4. Topography of Somma–Vesuvius and pyroclastic flows produced from the collapse of a plinian eruption column of Vesuvius.

4. Discussion

The main phase of a large-scale explosive eruption can last for several days and simulation of such an eruption is a very complex undertaking. This is because large computational resources are required to ensure that the physical–chemical–mathematical equations of the model are solved correctly (verification) and that

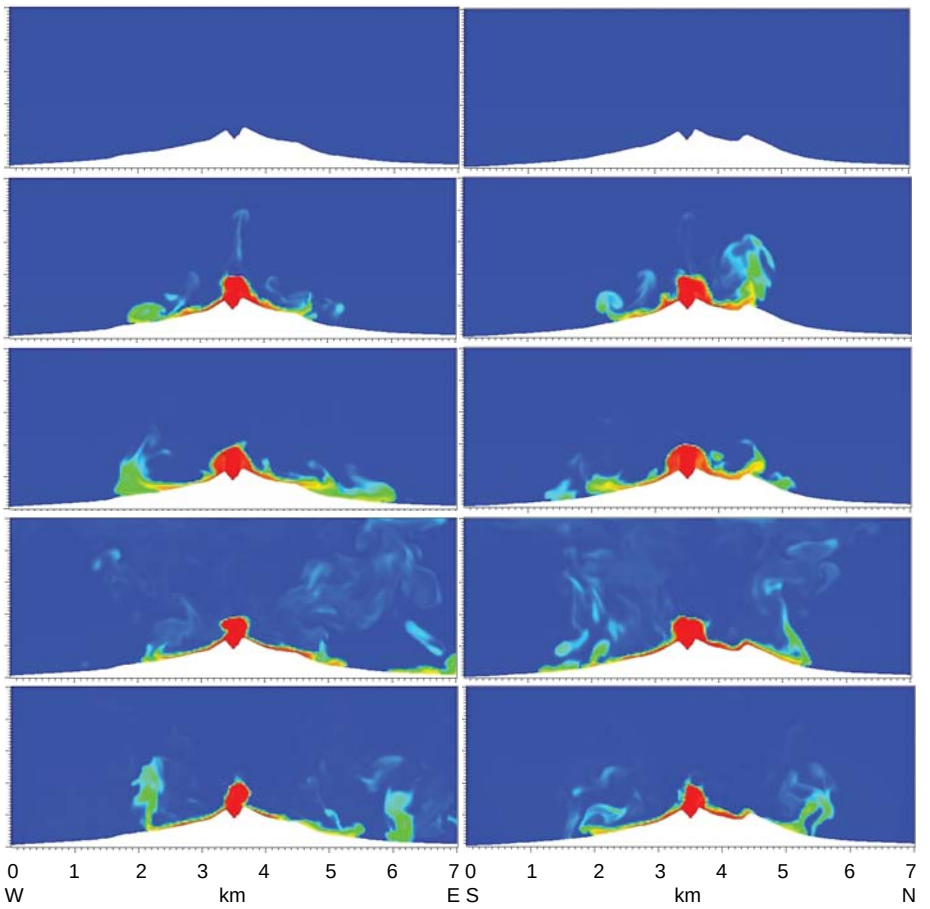

Figure 5. Temperature distributions along the WE and SN directions during the first minutes of an eruption of Vesuvius. The eruption produces column collapse and the pyroclastic flows propagate in different directions dependent of the topography and interactions of secondary columns produced on pyroclastic flows. The red color denotes temperature of about 1100 K and the blue color temperature of the atmosphere of about 300 K.

the model accounts for all relevant volcanic processes which can occur during the eruption (validation). For determining the effects of the eruptions on the built environment surrounding a volcano it is necessary to perform many simulations of different eruption scenarios to assess all possible hazards and their consequences that could be involved during the eruptions. And for producing resilient and sustainable habitats close to a volcano, these scenarios must also include those associated with the re-organization of the built environment, so that this environment can resist the eruptions with minimal socio-economic and

cultural losses [5, 17]. Reliable assessments of hazards and consequences of volcanic eruptions are necessary for ascertaining the vulnerability, risk, resilience, and sustainability of a city in the proximity of a volcano [18], but currently such assessments do not exist, because it is apparently easier to promote evacuation plans whose reliabilities are highly questionable and detrimental for producing resilience and sustainability of cities close to volcanoes [4].

The current development of Global Volcanic Simulator is aimed at simulating from start to finish not only the plinian eruptions of Vesuvius, but also the plinian and super eruptions of Campi Flegrei, in order to map as precisely as possible the exclusion, resilience, and sustainability areas of these volcanoes [5]. For Vesuvius discussed in this work, the exclusion and other areas are not uniformly distributed around the volcano, because of both the asymmetry of the volcanic edifice and the perturbing effects on the volcanic column caused by both the rotation of the Earth and local and global weather conditions. As shown in Fig. 5, even in the absence of such perturbations the topography of the volcano is sufficient to dramatically affect the propagation of pyroclastic flows, since Mt. Somma to the north of Vesuvius represents a significant barrier that slows down their propagations while Valle del Inferno between the cone of Vesuvius and Mt. Somma allows for an effective channeling of flows in the directions toward Pompei to the east and San Giuseppe Vesuviano and Naples to the west.

A plinian eruption produces a volcanic column that rapidly rises into the stratosphere and then distributes the ash over a wide area, and its partial and total collapses can affect the built environment around the volcano much more severely than the fall of cold ash from high rising volcanic plumes. The secondary *phoenix columns* produced on the pyroclastic flows are the result of competitions between different forces, since close to the volcanic vent the radial inertial forces dominate the vertical buoyancy forces, whereas farther away from the vent the opposite is true. The buoyancy forces can lift the material from the flows and transport it into the colder regions of the atmosphere where it cools and falls as ash to the ground at low temperatures. Simulations of complete eruptions are, therefore, necessary to understand the detailed behavior of these flows, because they propagate in waves and each wave can reach different distance from the vent [1].

The ability to simulate volcanic eruptions from the beginning to the end is crucial for reliably assessing the hazards from ash fall, pyroclastic flows, and lahars, since this provides the forces, moments, temperatures, and concentrations of materials at different times and locations in the environments surrounding the volcanos. This data, together with possible displacements, velocities, and accelerations of ground motions of built environments in the proximities of volcanoes, provide the necessary information for building the appropriate structures that can resist and protect the populations from eruption products. Building resilient and sustainable habitats around volcanoes requires integrations of several fields of science and collaboration of populations exposed to the hazards, which is, however, difficult to achieve in practice and in particular for large cities where there are many actors with different interests [9, 17].

5. Conclusions

A reliable Global Volcanic Simulator is a very useful tool for assessing multiple hazards from volcanoes, and in particular those in the Neapolitan area where there are several million people exposed to these hazards. If we want to build or make the existing cities close to volcanoes resilient and sustainable we must be able to produce reliable eruption scenarios for use in the urban planning of the territories, so that the populations can cohabit with the volcanoes in security and prosperity. The simulator discussed in this paper incorporates chemical and physical models of different parts of the volcano, and the current version can simulate magma chamber evolution, opening of volcanic conduits, steady-state and transient magma ascent in volcanic conduits with and without magma fragmentation, interaction of water in underground aquifers with magma in conduits, and dispersion of erupted materials in the atmosphere. Each model of the simulator is first verified and validated before being integrated with other models, and this integration is accomplished by a scheduler which ensures that the boundary conditions for all characteristic parts of the simulator work as effectively as possible, depending on the available computational resources. The current and future work on Global Volcanic Simulator is directed at both improving the current models, implementation of new models for simulating complete eruptions, and definitions of exclusion nuclei, resilience belts, and sustainability areas for the Neapolitan volcanoes.

References

1. Dobran, F. (2001). Volcanic Processes: Mechanisms in Material Transport. Springer, New York.
2. Cas, R.A.F., Wright, J.V. (1987). Volcanic Successions. Allen and Unwin, London.
3. Dobran, F., Barberi, F., Casarosa, C. (1990). Modeling of Volcanological processes and Simulation of Volcanic Eruptions. Giardini, Pisa.
4. Dobran, F. (2019). Vesuvius and Campi Flegrei Evacuation Plans: Implications for resilience and sustainability for Neapolitans. In Resilience and Sustainability of Cities in Hazardous Environments, F. Dobran (ed.). GVES, Napoli–New York.
5. Dobran, F. (2019). VESUVIUS–CAMPIFLEGREI PENTALOGUE: Resilience and sustainability framework for the Neapolitan area. In Resilience and Sustainability of Cities in Hazardous Environments, F. Dobran (ed.). GVES, Napoli–New York.
6. Dobran, F. (2007). Urban habitat construction around Vesuvius: Environmental risk and engineering chalenges. European Union COST 26 Project: Urban Habitat Constructions under Catastrophic Events, Prague 30-31 March 2007. http://http://www.gvess.org/Prague_2007_dobran.pdf (accessed 24 April 2018)
7. Roache, P.J. (1998). Verification and Validation in Computational Science and Engineering. Hermosa Publishers, Albuquerque, New Mexico.
8. Dobran, F. (1993). Global Volcanic Simulation of Vesuvius. Giardini, Pisa.
9. Dobran, F. (1994). Prospects for the global volcanic simulation of Vesuvius. Atti dei Convegni Lincei 112, 197-209. Accademia Nazionale dei Lincei, Roma.
10. Dobran, F. (1991). Theory of Structured Multiphase Mixtures. Springer-Verlag, New York.

11. Dobran, F., Ramos, J.I. (2006). Global volcanic simulation: Physical modeling, numerics, and computer implementation. In Vesuvius: Education, Security, and Prosperity, F. Dobran (ed.), 311-372. Elsevier, Amsterdam.
12. GVES (2018). Global Volcanic Simulator Manual: Edition 2018. GVES, Napoli–New York.
13. Hirschfelder, J.O., Curtis, C.F., Bird, R.B. (1954). Molecular Theory of Gases and Liquids. Wiley, New York.
14. Dobran, F. (1992). Modeling of structured multiphase mixtures. International Journal of Engineering Science 30, 1497-1505.
15. Santacroce, R. (1987). Somma-Vesuvius. CNR Quaderni 114, Roma.
16. Rosi, M., Principe, C., Vecci, R. (1993). The 1631 Vesuvius eruption: A reconstruction based on historical and stratigraphical data. Journal of Volcanology and Geothermal Research 53, 151-182.
17. Dobran, F. (2006). VESUVIUS 2000: Toward Security and Prosperity Under the Shadow of Vesuvius. In Vesuvius: Education, Security, and Prosperity, F. Dobran (ed.), 3-69. Elsevier, Amsterdam.
18. Dobran, F. (2019). Cities in hazardous environments: Risk assessment, resilience, and sustainability. In Resilience and Sustainability of Cities in Hazardous Environments, F. Dobran (ed.). GVES, Napoli–New York.